STRUCTURE, MORPHOLOGY AND HARDNESS OF A WAAM BUILT AL99.7 SPECIMEN

Georgi Kotlarski[1], Maria Ormanova[1], Alexander Nikitin[2], Ralf Ossenbrink[2], Nikolay Doynov[2,3], Stefan Valkov[1,4], Vesselin Michailov[2]

[1] Institute of Electronics, Bulgarian Academy of Sciences, 72 Tsarigradsko Chaussee, 1784 Sofia, Bulgaria

[2] Department of Joining and Welding Technology, Brandenburg University of Technology, Platz der Deutschen Einheit 1, 03046 Cottbus, Germany

[3] Institute of Metal Science, equipment, and technologies with Center for Hydro- and Aerodynamics, Bulgarian Academy of Sciences, 67 Shipchenski prohod Blvd., 1574 Sofia, Bulgaria

[4] Faculty of Mathematics, Informatics, and Natural Scineces, Technical University of Gabrovo, 4 H Dimitar Str., 5300 Gabrovo, Bulgaria

Abstract

The present work discusses the possibility of wire arc additive manufacturing (WAAM) of pure aluminum specimens (Al99.7). The manufactured specimen's structure was studied using X-ray diffraction (XRD) experiments. The morphology of the specimen at different stages of build-up was studied by examining pre-pared micrograph samples using an optical microscope. The resultant structure has a direct influence on the mechanical properties of the specimen, and for this reason the microhardness of the specimen was studied as well. The results of the present study were discussed regarding the change of the structure of the samples with the increase of the specimens' height during the manufacturing process and its' influence on the resultant microhardness.

Keywords: WAAM, Al99.7, structure, morphology, hardness.

INTRODUCTION

Wire arc additive manufacturing (WAAM) is a somewhat novel concept for manufacturing metallic components using a step-by-step component deposition. It is based on the already well known 3D printing technology used to produce polymeric components. There are a large number of variations of WAAM depending on the technological setup and the used materials. The most common one is that which employs gas metal arc welding (GMAW). The biggest advantages of this technology is the possibility of rapid high-accuracy formation of large size components with a complex physical shape and structure. This reduces the production costs by reducing the amount of post-processing needed after build-up [1].

Aluminum is a very highly sought after material due to its' lightweight structure and excellent mechanical properties such as high plasticity and strength. Usually it is implemented in structures and devices in different engineering fields in the form of alloys. The most commonly WAAM alloys known are Al5356, Al4043, Al4047, and more [2-4]. Pure aluminum such as Al99.5 and Al99.7 generally have no purpose in the field of mechanical engineering due to their poor corrosion and mechanical properties, however, a potential implementation in electrical systems may

be possible due to the high thermal and electrical conductivity of those materials.

The aforementioned advantages and disadvantages of Al99.5 and Al99.7 are the very reason why wire arc additive manufacturing of components using these materials is such a complicated and challenging task. Aluminum has a poor corrosion resistance which leads to the formation of aluminum oxide layers in the form of Al_2O_3 atop the surface of the components during the build-up process. This along with the high instability of the aluminum melt pool during the welding process due to the absence of stabilizing alloying agents leads to the formation of defects in the structure of the component such as pores and cracks.

Due to these challenges in the manufacturing of such components the present study observes the change in the structure of a WAAM built Al99.7 component as a function of the specimens' height and the resultant mechanical properties of the same, in particular, the microhardness.

EXPERIMENTAL SETUP

For the manufacturing of the component a KUKA KR15/1 robotic system was used with an EWM Alpha Q 552 MM RC welding unit. The welding wire used for the deposition process was Al99.7 with a thickness of 1.2 mm and a chemical composition as follows: < 0.20% Si, < 0.25% Fe, < 0.04% Cu, < 0.03% Mn, < 0.03% Mg, < 0.04% Zn, < 0.0003% Be, < 0.03% Ti, < 0.03% others, and balance Al. The specimen was deposited on an Al6061-T6 substrate with dimensions of 300 × 80 × 15 mm. The power of the welding arc was 2880 W, the wire feeding rate was 125 mm/s and the welding speed was 16 mm/s. The gas flow rate was 18 l/min, the wait time between the layers was 30 seconds in all cases and the offset between each consecutive layer was 1 mm.

Micrographic samples of the bottom, middle, and top sections of the specimen were prepared by means of mechanical polishing and etching using a 10 % solution of hydrofluoric acid (HF). The as prepared samples were examined using an optical microscope for the potential presence of any defects in the structure such as cracks are pores.

The samples were further examined using X-ray diffraction (XRD) in the symmetrical Bragg-Brentano mode with CuKα radiation of 1.54 Å. The obtained diffraction patterns were in the range of 30° to 80°. The phases detected during the experiment were identified using the International Centre for Diffraction Data (ICDD) database.

Each detected peak was fit using the SciDAVis 2.7 peak fitting software. The FWHM of the diffraction maxima was determined and the based on the obtained fits the lattice constant a (Å) of the samples was calculated using equation (1) used in the case of cubic structures.

$$a_{\{hkl\}} = d_{\{hkl\}} \cdot \sqrt{h^2 + k^2 + l^2} \qquad (1)$$

It is a function of the interplanar spacing d (Å) and the miller indexes {hkl} for the corresponding family of crystallographic planes.

The change in the texture of the samples was assessed by calculating the pole density $P_{\{hkl\}}$ of the obtained diffractograms using equation (2) which is proportional to the probability that a certain family of crystallographic planes is parallel to the surface.

$$P_{\{hkl\}} = \frac{\dfrac{I^{\exp}_{\{hkl\}}}{I^{st}_{\{hkl\}}}}{\left(\dfrac{1}{n}\right)\sum\left(\dfrac{I^{\exp}_{\{hkl\}}}{I^{st}_{\{hkl\}}}\right)} \cdot 100\% \qquad (2)$$

The pole density is a function of the experimentally obtained intensity ($I^{\exp}_{\{hkl\}}$) and the standard intensity of the peaks ($I^{st}_{\{hkl\}}$) given by the ICDD database of each family of crystallographic planes {hkl} related to the number of observed diffraction maxima n.

The Vickers hardness of the samples was obtained using a ZwickRoell Dura Scan 10/20 G5 microhardness tester with a diamond Vickers hardness indenter tip. The force used for the experiments in all cases was 1 N. The experiments were performed in agreement with the ISO 6507-2 standard.

RESULTS AND DISCUSSION

Fig. 1 presents optical images of the cross-section of the manufactured specimen. Fig. 1a presents a macro-image of the cross-section of the specimen, and Fig. 1b, 1c, and 1d present zoomed images of the cross-section of the top, middle, and bottom sections of the specimen, correspondingly. The average width of the specimen reached 9.0 ±0.3 mm. The low deviation off the mean value indicates a high accuracy of the deposition process. During the manufacturing process, 54 layers were deposited and the final height of the specimen was 51 mm, meaning that on average the thickness of each consecutive layer was 0.95 mm.

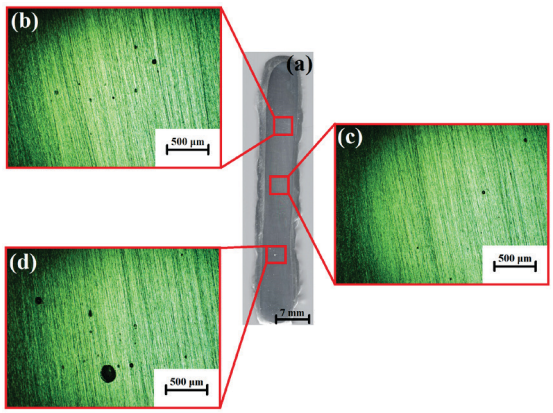

Fig. 1. *Optical images of the cross-section of the specimen (a), and the top (b), middle (c), and bottom (d) sections.*

The optical images of the different stages of specimen manufacturing indicate that a moderate amount of macro-pores are present. They may be attributed to the dynamic recovery processes that occur during the welding of the material or to the adsorption of gases in the weld pool. The most common theory as suggested by previous researchers [5] is that such macro-defects form in the structure of WAAM specimens due to the high adsorption of gases, particularly hydrogen, however, in the present work a definitive connection between the two phenomena cannot be established.

Fig. 2. once again presents optical images of the top, middle, and bottom sections of the specimens, taken however, using a higher level of zoom. A high quantity of scratches formed during the polishing process are noticeable, along with a certain concentration of micro-pores within the structure of the samples. The formation of such pores is usually connected to the compression of the metallic material during the solidification stage. This is why those pores are commonly referred to as solidification pores. The presence of such pores in WAAM build specimens, particularly using GMAW, is a common occurrence due to the high-energy input [6].

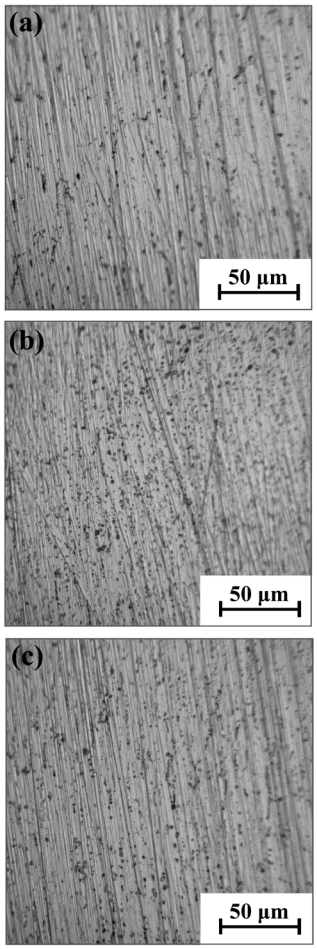

Fig. 2. *Optical images of the top (a), middle (b), and bottom (c) stages of build-up.*

A slight decrease of the concentration of solidification pores is visible at the top section of the specimen. Despite this, the presence of such defects theoretically reduces the hardness of the material [7].

The results of the performed XRD analysis are shown in Fig. 3. A highly polycrystalline structure of all samples is observed with an absence of amorphous halos. In all cases, a single-phase structure consisting of pure aluminum with a face-centered cubic (fcc) crystal structure is present. Planes corresponding to the {111}, {100}, {110}, and {311} families of planes were detected in the case of all samples.

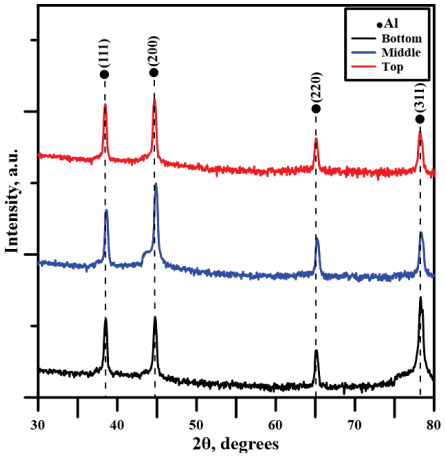

Fig. 3. *XRD patterns of the samples.*

The preferred crystallographic orientation of the samples is summarized in table 1 which represents the texture of the specimen. The $P_{\{hkl\}}$ at its' bottom and middle sections is 77.6 % and 76.9 % directed towards the {100} family of crystallographic planes, accordingly. The {100} family of planes characterizes with the lowest possible density and the lowest amount of slip planes in the cubic crystal lattice. The pole density $P_{\{hkl\}}$ at the top of the specimen was in the favor of the {311} family of planes with 60.7 %.

Table 1. Calculated pole density $P_{\{hkl\}}$ of the samples.

Sample	**$P_{\{hkl\}}$, %**				**FWHM {111}**
	$P_{\{111\}}$	$P_{\{100\}}$	$P_{\{110\}}$	$P_{\{311\}}$	
Bottom	6.0	14.0	2.4	77.6	2.266
Middle	7.7	76.9	5.6	9.8	2.137
Top	18.3	60.7	9.8	11.2	2.155

In order to gain more knowledge on the structure of the samples the FWHM was calculated using the above-mentioned software. The FWHM of the peak corresponding to the {111} family of planes at the bottom of the specimen was 2.266 ±0.034, at the middle it was 2.137 ±0.036, and at the top it was 2.155 ±0.051. Previous researchers have noticed that a decrease of the FWHM of the detected peaks corresponds to a parallel decrease of the defects in the crystal lattice [5]. However, no substantial difference between the FWHM of the peaks corresponding to the detected families of planes was observed, meaning that a somewhat uniform nature of the crystal structure was achieved.

The lattice constant of the samples was calculated according to equation (1). The calculated values were in all cases compared to the values indicated as standard for pure aluminum in the ICDD database which in the current case is 4.049 Å. No substantial difference in the values of the lattice parameter was observed following the direction of manufacturing of the specimen. The lattice constant at the bottom of the specimen was 4.046 Å, and towards the top of the specimen reached 4.042 Å.

In order to determine that Vickers hardness experiments were performed and the results are summarized in Fig. 4.

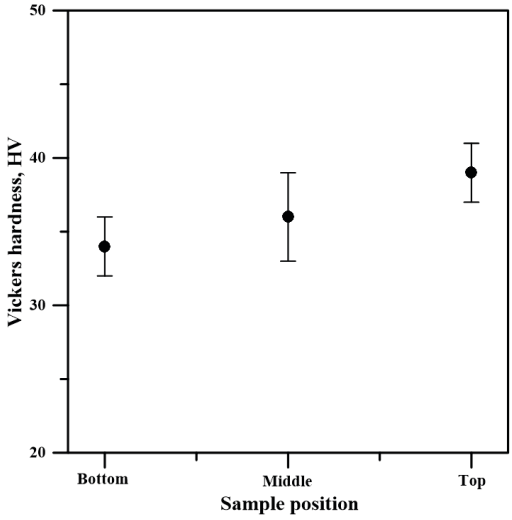

Fig. 4. *Vickers hardness of the samples.*

The bottom section of the specimen had a microhardness of 34 ±2 $HV_{0.1}$, the middle one had a microhardness of 36 ±3 $HV_{0.1}$, and the top one had a Vickers hardness of 39 ±2 $HV_{0.1}$. The obtained results indicate that no major increase of the microhardness was observed throughout the manufacturing process, however, a slight increase is indeed observed towards the top section of the specimen. The microhardness of all materials is directly affected by the structure of the studied samples. The primary reason for the change in the microhardness is the formation of solidification pores. Although they are donated as "solidification pores" the formation of such micro-defects does not necessarily relate only to the deformation of the material during the solidification stage, but also to the adsorption of gases which can also lead to such structural imperfections. It is general knowledge that gas adsorption increases with the increase of the temperature of the specimen, thus the interpass temperature. Theoretically, this means that an increase of the micro- or macro-defects should also be observed. Exactly the opposite trend was observed, which means that in the present case the most probable cause for the formation of micro-pores is the process of solidification.

CONCLUSIONS

The following conclusions can be derived from the current work:

- The applied technological conditions of layer deposition were sufficient enough to manufacture a pure aluminum specimen (Al99.7);
- The selected technological conditions did not lead to a significant change in the crystal structure of the specimen throughout the build-up process;
- The same amount of macro-pores was observed along the cross-section of the specimen;
- A slight decrease of the micro-pores was observed at the top of the specimen corresponding to a slight increase of the Vickers hardness;
- Although the hardness of the specimen changed slightly it remained about the same at all studied samples;
- The applied technological conditions were sufficient for the formation of a uniform specimen with nearly identical structure and microhardness.

The results of this work can suffice for the further optimization of WAAM of Al99.7 specimens using GMAW in the cold arc pulse mode and the formation of components with improved structure and mechanical properties, and a more complicated geometry.

ACKNOLEGEMENT

The financial support of the Bulgarian National Science Fund, grand number KP 06-DO 02/1 (2019) is greatly appreciated.

REFERENCE

[1] Wu B, Pan Z, Ding D, Cuiuri D, Li H, Xu J, Norrish J. A review of the wire arc additive manufacturing of metals: properties, defects and quality improvement. Journal of Manufacturing Processes 35 (2018) 127-139.

[2] Kohler M, Hensel J, Dilger K. Effects of Thermal Cycling on Wire and Arc Additive Manufacturing of Al-5356 Components. Metals 10 (2020) 952.

[3] Chakkravarthy V, Jerome S. Fabrication of preferentially oriented Al4043 alloy and its wear anisotropy. Materials Letters 280 (2020) 128578.

[4] Liu S, Wan D, Peng D, Lu X, Ren X, Fu Y, Wang F, Li Y, Zhang Zh, He J. Effect of heat input on Nanomechanical properties of wire-arc additive manufactured Al 4047 alloys. Materials Science and Engineering: A 860 (2022) 144288.

[5] Thapliyal S. Challenges associated with the wire arc additive manufacturing (WAAM) of aluminum alloys. Materials Research Express 6 (2019) 112006.

[6] Kerekar K, Lawrence J, Melton G, Addison A, Zhang X, Xu L. Influence of Interpass Temperature on Wire Arc Additive Manufacturing (WAAM) of Aluminum Alloy Components. MATEC Web of Conferences 269 (2019) 05001.

[7] Kohler M, Hensel J, Dilger K. Effects of Thermal Cycling on Wire and Arc Additive Manufacturing of Al-5356 Components. Metals 10 (2020) 952.